Structure and Dynamics of Micelle-Associated Human Immunodeficiency Virus gp41 Fusion Domain[†,‡]

Christopher P. Jaroniec,*,§ Joshua D. Kaufman,‖ Stephen J. Stahl,‖ Mathias Viard,⊥ Robert Blumenthal,⊥ Paul T. Wingfield,‖ and Ad Bax*,§

Laboratory of Chemical Physics, National Institute of Diabetes and Digestive and Kidney Diseases, and Protein Expression Laboratory, National Institute of Arthritis and Musculoskeletal and Skin Diseases, National Institutes of Health, Bethesda, Maryland 20892, and Center for Cancer Research Nanobiology Program, National Cancer Institute, National Institutes of Health, Frederick, Maryland 21702

ABSTRACT: The N-terminal fusion domain of the HIV-1 gp41 envelope glycoprotein is responsible for initiating the fusion of viral and cellular membranes, leading to the subsequent infection of the host cell by HIV-1. We have investigated the backbone structure and dynamics of the 30 N-terminal residues of HIV-1 gp41 in membrane-mimicking environments using NMR spectroscopy and ^{15}N- and ^{15}N,^{13}C,^{2}H-labeled peptides. Similar ^{15}N−^{1}H HSQC spectra were obtained in a variety of detergents, including SDS, DPC, mixed DPC/SDS, and LPPG micelles, indicating that the peptide structure is not strongly influenced by the type of detergent used. Detailed characterization was carried out in SDS micelles, where the long-term sample stability was found to be optimal. In addition to *J*-coupling and NOE restraints, a nearly complete set of backbone residual dipolar coupling restraints was recorded for the fusion domain−micelle complex aligned with respect to the magnetic field using a stretched polyacrylamide gel. Backbone amide ^{15}N spin relaxation and amide hydrogen exchange rates with the solvent were also measured. The ensemble of NMR structures reveals an uninterrupted α-helix for the least mobile residues ($S^2 > 0.65$), Ile-4 to Met-19, with transient helical character extending up to Ala-22. A 12-residue (Ile-4 to Ala-15) segment is fully shielded from solvent, with Gly-3 and Gly-16 found at micelle−solvent interfaces. Residues external to the micelle exhibit enhanced picosecond to nanosecond time scale dynamics relative to the residues buried in the micelle, and their mobility increases with the distance from the micelle.

Enveloped viruses, such as the human immunodeficiency virus type 1 (HIV-1),[1] influenza virus, and other members of diverse viral families including retro-, filo-, paramyxo-, and orthomyxoviruses, express surface glycoproteins, which mediate the attachment and fusion of viral and cellular membranes leading to the release of viral contents into the host cell and subsequent infection (*1−5*). Despite differences in amino acid sequence, details of the three-dimensional structure, and precise mode of entry (e.g., direct fusion at the plasma membrane for HIV-1 versus endocytosis followed by fusion at low pH for influenza virus), at the molecular level viral glycoproteins display a number of common features and appear to employ a similar mechanism for entering the host cell. Viral envelope glycoproteins are typically assembled as homotrimers (*6−16*) and are proteolytically cleaved into two subunits, a receptor-binding subunit and a fusion subunit anchored in the viral membrane (*2*, *3*). For the influenza virus these correspond to subunits

* To whom correspondence should be addressed. C.P.J.: National Institutes of Health, Building 5, Room B1-27, 9000 Rockville Pike, Bethesda, MD 20892-0520. Phone: (301) 496-7098. Fax: (301) 496-0825. E-mail: jaroniec@speck.niddk.nih.gov. A.B.: National Institutes of Health, Building 5, Room 126, 9000 Rockville Pike, Bethesda, MD 20892-0520. Phone: (301) 496-2848. Fax: (301) 402-0907. E-mail: bax@nih.gov.

§ National Institute of Diabetes and Digestive and Kidney Diseases.
‖ National Institute of Arthritis and Musculoskeletal and Skin Diseases.
⊥ National Cancer Institute.

[1] Abbreviations: aa, amino acid; AA, acrylamide; AMPS, 2-(acrylamido)-2-methyl-1-propanesulfonic acid; BIS, bis(acrylamide); DOPC, dioleoylphosphatidylcholine; DOPE, dioleoylphosphatidylethanolamine; DPC, dodecylphosphocholine; EPR, electron paramagnetic resonance; FID, free induction decay; FMOC, 9-fluorenylmethoxycarbonyl; gp, glycoprotein; gp41$^{1−N}$, peptide corresponding to residues $1−N$ of the HIV-1 gp41 protein; HA, hemagglutinin; HIV-1, human immunodeficiency virus type 1; HPLC, high-performance liquid chromatography; HSQC, heteronuclear single-quantum correlation; IPAP, in-phase antiphase; KSI, ketosteroid isomerase; LPPG, 1-palmitoyl-2-hydroxy-*sn*-glycero-3-phospho-*rac*-1-glycerol; LUV, large unilamellar vesicles; MALDI, matrix-assisted laser desorption/ionization; MFR, molecular fragment replacement; NMR, nuclear magnetic resonance; N-NBD-PE, *N*-(7-nitrobenz-2-oxa-1,3-diazol-4-yl)phosphatidylethanolamine; NOE, nuclear Overhauser effect; N-Rh-PE, *N*-(lissamine rhodamine B sulfonyl)phosphatidylethanolamine; PAGE, polyacrylamide gel electrophoresis; PCR, polymerase chain reaction; RDC, residual dipolar coupling; RET, resonance energy transfer; rms, root mean squared; SA, simulated annealing; SDS, sodium dodecyl sulfate; SIV, simian immunodeficiency virus; TEMED, *N,N,N′,N′*-tetramethylethylenediamine; TOF, time of flight; wt, wild type; 1D, one dimensional; 2D, two dimensional; 3D, three dimensional.

of the hemagglutinin (HA) glycoprotein, HA1 and HA2, respectively, which are covalently linked via a disulfide bond, whereas for HIV-1 the receptor-binding subunit, gp120, is noncovalently associated with the transmembrane subunit, gp41 (*2*, *3*).

The entry of HIV-1 into host cells involves the initial binding of gp120 to the CD4 glycoprotein (*17*) and a chemokine coreceptor, primarily CCR5 or CXCR4 (*18*), on the cell surface. This is believed to be followed by conformational changes in gp120 and gp41, resulting in the exposure toward the cell membrane of a highly hydrophobic sequence of 20−30 N-terminal amino acids of gp41, termed the fusion domain or fusion peptide (*2*, *3*). The subsequent insertion of the fusion peptide into the cell membrane enables gp41 to simultaneously span the viral and cell membranes and initiates the fusion process, which eventually leads to the mixing of viral and cell membrane lipids and the formation of a fusion pore through which the viral contents are incorporated into the host cell. The membrane fusion process proceeds through a series of steps, the precise sequence and details of which are not completely understood but which involves the dissociation of gp120 from the membrane-anchored gp41 and the rearrangement of gp41 into a fusion-active conformation (*2*, *3*).

Although no atomic resolution structure is available for the native, prefusion conformation of HIV-1 gp41, several high-resolution structures have been determined for the extremely stable, fusion-active ectodomain of this protein (*8*−*10*) and that of the closely related simian immunodeficiency virus (SIV) gp41 (*11*−*13*). These structures reveal a bundle of six α-helices: a coiled-coil core consisting of three, so-called, N-terminal helices, i.e., immediately adjacent to the N-terminus of gp41 and the fusion peptide, with three C-terminal helices, i.e., those closer to the C-terminus of gp41, arranged on the outside of the coiled-coil core and oriented antiparallel relative to the N-terminal helices. Such a structure places the fusion peptide in the vicinity of the viral transmembrane anchor, which is consistent with the proposed fusion-active and postfusion conformations of gp41 (*2*, *3*). Interestingly, similar trimeric coiled-coil core structures have been observed for other glycoproteins representing diverse viral families (*6*, *7*, *14*−*16*), indicating that different viruses may employ a similar mechanism to accomplish membrane fusion.

Due to the reduced solubility of protein constructs containing the N-terminal fusion peptide (*19*), high-resolution structures of ectodomains of viral fusion proteins have been determined for constructs lacking the fusion domain (*6*−*16*). At the same time the importance of the highly conserved N-terminal domains in mediating viral membrane fusion is widely recognized (*1*−*5*, *20*−*22*). Indeed, ectodomains and fusion peptides are believed to form independently folded domains (*23*), and even relatively conservative point mutations can have dramatic effects on fusion activity (*20*−*22*, *24*−*29*). Moreover, short, synthetic peptides mimicking the N-terminal fusion domains have been shown to be capable of promoting lipid mixing and membrane fusion (*20*−*22*, *30*−*32*). Consequently, synthetic fusion peptides reconstituted into lipid bilayers, detergent micelles, and other membrane mimetics have become model systems of choice for gaining further insight into the structural basis of viral membrane fusion (*20*−*22*) and have been characterized using

a variety of biophysical techniques, including solution- and solid-state nuclear magnetic resonance (NMR), electron paramagnetic resonance (EPR), infrared spectroscopy, circular dichroism, and molecular dynamics simulations. These studies indicate that fusion domains of the influenza virus and HIV-1 exhibit significant plasticity and can adopt either α-helical or oligomeric β-strand conformations (*20*−*22*, *32*−*45*). Factors such as the peptide to lipid ratio, lipid composition, and presence of cholesterol in the membrane mimetic have been identified as significant determinants of conformational preferences, with lower peptide to lipid ratios typically favoring helical conformations (*20*−*22*), and a recent study notes that both helical and β-strand conformations are fusion-active in lipid mixing assays (*43*). Thus, detailed characterization of fusion domains of viral fusion glycoproteins under various membrane-mimicking conditions remains a topic of significant interest.

Solution-state NMR techniques can provide a large number of site-specific geometric restraints required for de novo determination of three-dimensional structure as well as information about molecular dynamics, and these methods have been applied extensively to the characterization of fusion peptides (*35*, *40*, *42*) and other membrane peptides and proteins (*46*−*58*) reconstituted into detergent micelles. For the influenza HA fusion domain a detailed NMR study of a "host−guest" peptide [consisting of a 20-residue HA fusion domain and a GCGKKKK solubility enhancement tag (*39*)] in dodecylphosphocholine (DPC) micelles, combined with EPR measurements, showed that under both neutral (pH 7.4) and fusogenic (pH 5) conditions the peptide adopts distinct helical, highly amphipathic, inverted "V" structures (*40*). In the case of HIV-1, however, 2D ^{1}H NMR and spin-label studies of a model 23-residue fusion peptide from the LAV$_{1a}$ strain of HIV-1 gp41 have arrived at somewhat inconsistent conclusions (*35*, *42*). Although both studies show that the HIV-1 gp41 fusion domain adopts a primarily helical conformation in complex with a detergent micelle, results in negatively charged sodium dodecyl sulfate (SDS) micelles were interpreted in terms of the presence of a type I β-turn formed by residues Ser-17 to Gly-20 and indicated significant interactions of the C-terminal residues with the micelle surface (*35*), while measurements in zwitterionic DPC micelles indicated a more regular helical conformation protruding from the micelle into the solvent (*42*); neither study addressed, in detail, the question of peptide backbone or side-chain dynamics. It is not clear a priori whether the reported structural differences are due to different lipid headgroups or other factors. However, by analogy to the influenza HA fusion domain, where relatively subtle changes in three-dimensional structure between neutral and fusion-active conformations were implicated to have functional relevance (*23*, *40*), the fine details of structure and dynamics of the HIV-1 gp41 fusion domain are also likely to be important for the membrane fusion process.

In this paper we present the three-dimensional structure and dynamics of the HIV-1 gp41 fusion domain, as determined by solution-state NMR in detergent micelles. NMR spectra of the fusion domain were recorded in a variety of membrane mimetics including SDS, DPC, mixed DPC/SDS, and 1-palmitoyl-2-hydroxy-*sn*-glycero-3-phospho-*rac*-1-glycerol (LPPG) micelles, and detailed characterization was carried out in SDS micelles where the long-term sample

stability was found to be optimal. The peptide construct used included 30 N-terminal residues of HIV-1 gp41, i.e., the consensus fusion peptide sequence and the region of HIV-1 gp41 linking the fusion peptide to the stable ectodomain, and a highly charged solubility enhancement tag in analogy to the host−guest system employed by Tamm and co-workers in the recent studies of the influenza HA fusion domain (*39*, *40*). In addition to an extensive set of site-specific $^3J_{HNH\alpha}$-coupling and NOE restraints (*59*), a nearly complete set of backbone residual dipolar coupling (RDC) restraints (*60*, *61*) was recorded for the fusion domain−micelle complex, aligned with respect to the magnetic field using a stretched polyacrylamide gel (*62*−*64*). Side-chain conformations and χ^1 rotamer averaging were also investigated (*65*, *66*). Backbone dynamics were probed by measuring site-specific ^{15}N spin relaxation parameters, and measurements of exchange of amide protons with the solvent were used to provide information about the stability of hydrogen bonds and the location of the fusion domain with respect to the micelle.

MATERIALS AND METHODS

Materials. Sodium dodecyl sulfate (SDS) was purchased from Quality Biological, Inc. (Gaithersburg, MD) as a 10% aqueous solution. [^{13}C]Glucose, $^{15}NH_4Cl$, D_2O, and deuterated SDS (SDS-d_{25}) were purchased from Cambridge Isotope Laboratories (Andover, MA). Dodecylphosphocholine (DPC), 1-palmitoyl-2-hydroxy-*sn*-glycero-3-phospho-*rac*-1-glycerol (LPPG), dioleoylphosphatidylcholine (DOPC), dioleoylphosphatidylethanolamine (DOPE), and the fluorescent probes *N*-(7-nitrobenz-2-oxa-1,3-diazol-4-yl)phosphatidylethanolamine (N-NBD-PE) and *N*-(lissamine rhodamine B sulfonyl)phosphatidylethanolamine (N-Rh-PE) were purchased from Avanti Polar Lipids, Inc. (Alabaster, AL). Wang resin was obtained from Peptides International (Louisville, KY), and FMOC-protected amino acids were from Novabiochem (San Diego, CA) and Midwest Biotech, Inc. (Fishers, IN). Cholesterol and reduced Triton X-100 were obtained from Sigma (St. Louis, MO). All other reagents were of analytical grade.

Synthesis of HIV-1 gp41$^{1-23}$ Fusion Peptides for Lipid Mixing Assays. To assess the influence of an N-terminal Pro residue, absent in wt HIV-1 gp41 but present in the gp41$^{1-30}$ construct used for the NMR studies (see below), on the fusion activity of the HIV-1 gp41 fusion domain, we synthesized two peptides: a control peptide, gp41$^{1-23}$, consisting of the 23 N-terminal residues of HIV-1 gp41 (AVGIGALFLGFLGAAGSTMGAAS), and a 24-residue peptide, P-gp41$^{1-23}$. The peptides were synthesized on a Perkin-Elmer/Applied Biosystems model 433A solid-phase peptide synthesizer using standard FMOC synthesis and cleavage protocols. Amino acid analysis and MALDI-TOF mass spectrometry were used to verify peptide purity.

Lipid Mixing Assay for Membrane Fusion. Large unilamellar vesicles (LUV) consisting of DOPC, DOPE, and cholesterol (molar ratio, 1:1:1) were prepared by extrusion (*67*). The lipids were dissolved in chloroform and then dried under a stream of nitrogen. Excess solvent was removed by overnight lyophilization. Dry lipid films were suspended in PBS buffer by vortexing to produce large multilamellar vesicles. The lipid suspension was further processed with six cycles of freezing and thawing followed by 20 extrusions through polycarbonate membranes with 0.1 μm diameter pores to generate LUV.

Membrane lipid mixing was monitored using the resonance energy transfer (RET) assay, described by Struck et al. (*68*). Measurements were conducted at 37 °C in thermostatically controlled cuvettes using a SLM-Aminco (Urbana, IL) spectrofluorometer. The medium in the cuvettes was continuously stirred to allow the rapid mixing of HIV-1 gp41$^{1-23}$ peptides and vesicles. The peptides were added as small aliquots of a 1 mM solution in DMSO, to a final peptide concentration of 8−32 μM (see Figure 2 legend). The assay is based on the dilution of N-NBD-PE and N-Rh-PE. Dilution due to membrane mixing results in an increase in N-NBD-PE fluorescence. Vesicles containing 0.6 mol % of each probe were mixed with unlabeled vesicles at a 1:4 ratio. The NBD emission was monitored at 530 nm with the excitation wavelength set at 465 nm. A cutoff filter at 515 nm was used between the sample and the emission monochromator to avoid scattering interferences. The fluorescence scale was calibrated such that the zero level corresponded to the initial residual fluorescence of the labeled vesicles and the 100% value to complete mixing of all of the lipids in the system (obtained by adding reduced Triton X-100). The final lipid concentration was 3 mM.

Expression and Purification of HIV-1 gp41$^{1-30}$ Fusion Peptides for NMR Studies. The fusion protein construct consisted of (His)$_6$-KSI(D38A)-GGGGSDP-gp41$^{1-30}$-DYKDDDDK, where (His)$_6$ is the polyhistidine tag; KSI, the 125 aa ketosteroid isomerase with a D38A mutation inserted to stabilize the protein during partial acid cleavage; GGGGSDP, the Asp−Pro acid cleavage site (*69*); gp41$^{1-30}$, residues 1−30 of the HIV-1 gp41 protein (see Figure 1); and DYKDDDDK, the flag epitope (*70*) used to improve the peptide solubility (*39*), which we found to be essential for successful chromatographic purification. This plasmid was constructed by generating all but the last three codons of the KSI(D38A) portion of the protein as a *Nde*I−*Mlu*I DNA fragment using the PCR technique of Scharf et al. (*71*) with pET-31b(+) (Novagen, Madison, WI) as the template DNA. The internal Asp−Pro site in the KSI moiety had been previously eliminated by changing Asp-38 to Ala using the technique of Vallette et al. (*72*). The ACQ-GGGGSDP-gp41$^{1-30}$-DYKDDDDK coding sequence was generated as a *Mlu*I−*Bam*HI fragment, again using the PCR technique of Scharf et al. (*71*) with a plasmid DNA containing the HIV-1 gp41 gene as the template DNA. These two fragments were inserted between the *Nde*I and *Bam*HI sites of plasmid pET28a(+) (Novagen) to generate the fusion protein construct.

Fermentation of the plasmid in BL21(DE3) cells and labeling with ^{15}N or ^2H, ^{15}N, and ^{13}C were performed using a BIOSTAT series B benchtop fermentor (Sartorius BBI Systems, Bethlehem, PA) using minimal media as previously described (*73*). The cells were induced at OD$_{600}$ ≈ 4.0 with 0.5 g of IPTG (2 mM) at 37 °C for 3 h. The fermentation yield was typically 25 g of cells (wet weight).

Cell breakage and preparation of inclusion body protein were as previously described (*73*). The insoluble fusion protein was extracted with guanidine hydrochloride and purified by metal chelate chromatography and gel filtration. The (His)$_6$-tagged KSI moiety was cleaved from the peptide

using 10% formic acid at 80 °C for 90 min. The peptide was purified by gel filtration and reverse-phase HPLC, and its mass and purity were assayed using an Agilent 1100 LC/MSD mass spectrometer. The concentration of the purified peptide was measured by absorbance at 280 nm (1 mg/mL = 0.309). Purified peptide was lyophilized and dissolved in detergent containing solvents for NMR analysis (see below).

NMR Sample Preparation. Samples were prepared by dissolving ^{15}N- or ^{15}N,^{13}C,^{2}H-labeled lyophilized peptides at a concentration of 0.7 mM in an H$_2$O solution containing 75 mM SDS (or other detergents; see Supporting Information for details), 7% D$_2$O, and 0.05% (w/v) NaN$_3$ in a total volume of 300 μL. Note that SDS-d_{25} was used to reconstitute the ^{15}N-labeled peptides. In all cases 25 mM NaH$_2$PO$_4$/Na$_2$HPO$_4$ buffer was used to maintain the pH at 6.5, except for the two ^{15}N-labeled samples used to investigate amide proton exchange with the solvent, where the pH was adjusted to 5.8 and 7.2 by the addition of HCl and NaOH, respectively. Isotropic samples were transferred to Shigemi microcells (Shigemi Inc., Allison Park, PA), and the field-aligned sample was prepared as described below.

For the RDC measurements the fusion peptide−micelle complex was oriented in a negatively charged polyacrylamide gel (62−64, 74, 75) as follows. The gel was polymerized from a solution of 5.51% (w/v) acrylamide (AA)/2-(acrylamido)-2-methyl-1-propanesulfonic acid (AMPS)/bis(acrylamide) (BIS) (4.02% AA, 1.35% AMPS, 0.14% BIS), 0.1% (w/v) ammonium persulfate, and 0.33% (v/v) *N,N,N′,N′*-tetramethylethylenediamine (TEMED) in 100 mM Tris-HCl buffer at pH 8.0. The above solution (300 μL) was transferred to a 5.7 mm diameter cylinder and allowed to polymerize for 4 h. The polymerized gel was washed in 50 mL of 50 mM NaH$_2$PO$_4$/Na$_2$HPO$_4$ buffer at pH 6.5 for 12 h, followed by two 12 h washes in 50 mL of H$_2$O. The gel was then dehydrated for about 40 h at 37 °C to a volume of ca. 10−20 μL and subsequently soaked for 48 h in 300 μL of the ^{15}N,^{13}C,^{2}H-labeled fusion peptide solution described above. The gel containing the fusion peptide−micelle complex was transferred into a 5.7 mm cylinder and compressed to a final diameter of 4.24 mm (i.e., axially stretched by a factor of ca. 1.8) by forcing it through a connecting funnel into an open-ended NMR tube (New Era Enterprises, Inc., Vineland, NJ) as described previously (64). The tube was sealed on the bottom using a plug fitted with an O-ring (New Era Enterprises, Inc.) and on top using a Shigemi plunger (64). The gel was allowed to equilibrate in the NMR tube for 12 h and exhibited a constant solvent ^{2}H quadrupolar splitting of 3.5 Hz throughout the NMR measurements.

At the peptide and SDS concentrations employed in this work the isotropic samples were stable over a period of at least 4 weeks, while significant peptide aggregation occurred within ca. 10 days for the field-aligned sample. By comparison, isotropic samples prepared in DPC, mixed SDS/DPC, or LPPG micelles (see Supporting Information, Figure S3) exhibited significantly reduced initial spectral intensities and sample lifetimes relative to SDS micelles, with significant peptide aggregation taking place within ca. 4 days.

NMR Spectroscopy. All experiments were carried out at 25 °C using Bruker spectrometers operating at ^{1}H Larmor frequencies of 600, 750, and 800 MHz and equipped with triple resonance three-axis pulsed field gradient room temperature or triple resonance *z*-gradient cryogenic probes,

optimized for ^{1}H detection. Data were processed using NMRPipe (76) and analyzed using the NMRPipe package and Sparky (77). H^N, N, C′, C$^\alpha$, and C$^\beta$ resonance assignments were obtained using a set of 3D triple resonance experiments: HNCO, HNCA, HN(CO)CA, and HN(CA)-CB, optimized for ^{2}H,^{13}C,^{15}N-labeled proteins and based on the pulse schemes of Yamazaki et al. (78). H$^\alpha$ and partial side-chain ^{1}H assignments were obtained using 3D ^{15}N-TOCSY-HSQC (79) recorded on the ^{15}N-labeled sample with TOCSY mixing times of 48 and 83 ms.

NOEs between H^N and other protons were measured using 3D ^{15}N-NOESY-HSQC (79) recorded on the ^{15}N-labeled sample with a NOESY mixing time of 100 ms. $^3J_{HNH\alpha}$ couplings were measured on the ^{15}N-labeled sample using the 3D HNHA experiment (80). Two-dimensional spin−echo difference experiments which probe $^3J_{NC\gamma}$ and $^3J_{C'C\gamma}$ couplings in aromatic residues (65) and $^3J_{NC\gamma}$ couplings in aliphatic residues (66) were recorded on the ^{15}N,^{13}C,^{2}H-labeled sample.

$^1J_{NH}$, $^1J_{NC'}$, $^1J_{C'C\alpha}$, and $^1J_{C\alpha C\beta}$ couplings, where $^1J_{IS}$ corresponds to $^1J_{IS}$ and $^1J_{IS} + {}^1D_{IS}$ in isotropic and field-aligned ^{15}N,^{13}C,^{2}H-labeled samples, respectively, were determined using a combination of 2D ^{1}H−^{15}N IPAP-HSQC (81) and semiconstant time H^N-coupled 3D HNCO, quantitative *J*-correlation 3D HNCO (82), C$^\alpha$-coupled 3D HNCO (83), and C$^\beta$-coupled 3D HN(CO)CA (84) experiments, respectively.

The ^{15}N relaxation parameters R_1 and R_2 and $\{^1H\}-{}^{15}$N NOE were measured at 60.8 MHz ^{15}N Larmor frequency using the ^{15}N-labeled sample and pulse schemes previously published by Farrow et al. (85). For the R_1 and R_2 measurements relaxation delays of 1 s were employed; for the $\{^1H\}-{}^{15}$N NOE measurement a 5 s relaxation delay and a 1 s relaxation delay followed by a 4 s proton presaturation period were used for the reference and NOE spectra, respectively. The exchange of amide protons with the solvent was investigated for ^{15}N-labeled fusion peptide samples at pH 5.8 and 7.2 by measuring peak intensities in 2D ^{1}H−^{15}N HSQC spectra recorded with and without presaturation of the water resonance during a 1.5 s relaxation delay (86).

Structure Calculations. An ensemble of 30 structures for the micelle-bound HIV-1 gp41 fusion domain consistent with the TALOS-derived (87) dihedral, $^3J_{HNH\alpha}$, NOE, and RDC restraints was generated using the simulated annealing (SA) molecular dynamics protocol implemented in the program Xplor-NIH 2.9.4 (88). A random coil peptide was used as the initial structure in the calculations, and each subsequent SA trajectory used as its input structure the output structure from the previous run (note that essentially identical results were obtained for different initial structures). Each SA trajectory was 400 ps long with the temperature linearly ramped from the initial value of 2000 K to 1 K in 10 K increments. The potential energy function included the standard bond, angle, and improper torsion angle terms. In addition, a quartic repulsive-only nonbonded potential was used, with atomic radii scaled down from their van der Waals values by a factor of 0.82. The potential energy terms corresponding to the NOE, dihedral, and $^3J_{HNH\alpha}$ restraints were held fixed at 5 kcal/Å^2, 100 kcal/rad^2, and 1 kcal/Hz^2, respectively, during the entire SA trajectory, while terms corresponding to RDC restraints (all RDCs were normalized with respect to a one-bond ^{15}N−^{1}H dipolar coupling, D^{NH})

```
         1     5      10        15        20
     P AVGIGALFLG FLGAAGSTMG

        25       30        35
     AASMTLTVQA DYKDDDDK
```
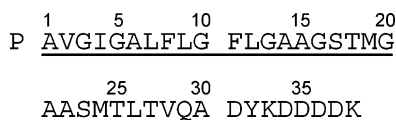
FIGURE 1: Amino acid sequence of the HIV-1 gp41 fusion domain construct used for the NMR studies. The peptide consists of (i) the N-terminal Pro residue derived from an Asp−Pro acid cleavage site found in the KSI fusion protein construct used to express isotopically labeled gp41$^{1-30}$ (see Materials and Methods section), (ii) 30 N-terminal residues of HIV-1 gp41 (underlined) labeled as Ala-1 through Ala-30, and (iii) the C-terminal flag epitope, DYKDDDDK, which acts as a solubility enhancement tag.

were ramped from 0.001 to 0.2 kcal/Hz^2 in the standard fashion. The potential profiles were of the soft-square and flat-well harmonic types for the NOE and dihedral restraints, respectively. For the *J*-coupling and RDC restraints regular harmonic potentials were used. To minimize the influence of backbone dynamics on the calculated structures, RDC restraints were included only for the least mobile residues, I4−M19, which exhibited generalized order parameters of $S^2 > 0.65$ based on ^{15}N spin relaxation measurements. In an attempt to further compensate for the influence of dynamics on the measured RDCs, the RDCs were scaled by a factor of $(S^2)^{-1/2}$ in a residue-specific fashion according to the generalized order parameter measured for each residue. In addition, dihedral restraints were available for residues I4−A22, and NOE and $^3J_{HNH\alpha}$ restraints were available for residues V2−M24. Consequently, residues A1−G3 and S23−A30, which exhibit enhanced picosecond to nanosecond time scale dynamics and appear to adopt random coil conformations based on the observed chemical shifts, are essentially unrestrained in the calculations. Finally, we note that no experimental dihedral restraints were included for the side chains, since $^3J_{NC\gamma}$ and $^3J_{C'C\gamma}$ coupling measurements indicate rapid χ^1 rotamer averaging throughout the entire peptide (see Supporting Information, Figure S5).

RESULTS

Influence of the N-Terminal Pro Residue on HIV-1 gp41 Membrane Fusion. The biosynthetic preparation of the ^{15}N- and ^{15}N,^{13}C,^{2}H-labeled HIV-1 gp41 fusion domain for NMR characterization was accomplished by the use of a fusion protein construct having an internal Asp−Pro acid cleavage site (see Materials and Methods section). The final fusion domain construct used for the NMR studies (P-gp41$^{1-30}$-DYKDDDDK; Figure 1) places a Pro residue at the N-terminus of gp41$^{1-30}$ in addition to having a C-terminal DYKDDDDK flag epitope, used for improved solubility. On the basis of previous studies (e.g., ref *43*), where the effect of C-terminal solubility enhancement tags on the activity of model fusion peptides was investigated using lipid mixing assays, the flag epitope is expected to have minimal influence on lipid mixing and membrane fusion. However, the effect of a non-native Pro residue at the N-terminus of gp41$^{1-30}$ on the fusion activity is not clear a priori, since the ability of HIV-1 gp41 to promote membrane fusion can be severely attenuated or even completely abolished by single amino acid mutations within the first 20−30 residues (*28*).

To assess whether the additional Pro residue significantly influences the fusion activity of the P-gp41$^{1-30}$-DYKDDDDK construct used for the NMR studies, lipid mixing assays were performed using two synthetic model peptides: a control
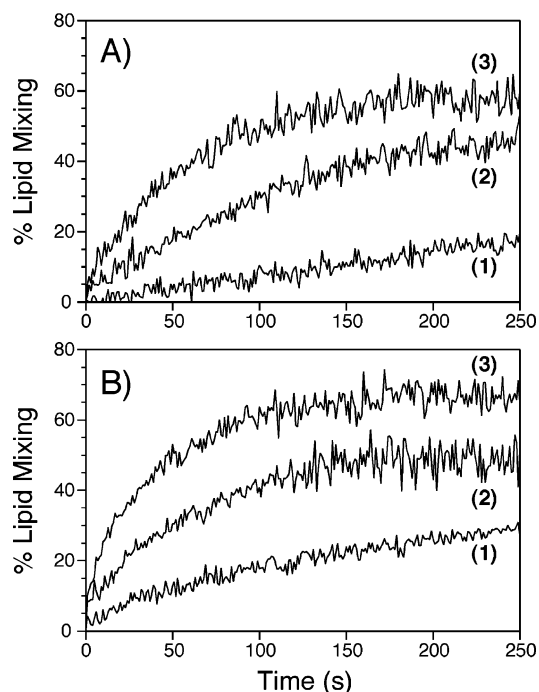
FIGURE 2: Lipid mixing induced by a peptide corresponding to the 23 N-terminal residues of HIV-1 gp41 (gp41$^{1-23}$) (A) and a peptide consisting of a Pro residue followed by gp41$^{1-23}$ (P-gp41$^{1-23}$) (B). Lipid mixing was induced with approximately (1) 8 μM, (2) 16 μM, and (3) 32 μM gp41$^{1-23}$ or P-gp41$^{1-23}$. See Materials and Methods section for additional details of the lipid mixing assay.

peptide, HIV-1 gp41$^{1-23}$, well-known to promote lipid mixing and membrane fusion (*38*, *43*), and a 24-residue peptide, P-gp41$^{1-23}$. The results in Figure 2 show that upon addition of aliquots of gp41$^{1-23}$ or P-gp41$^{1-23}$ to LUV nearly identical profiles of lipid mixing are observed and thus clearly indicate that the N-terminal Pro residue has no adverse effect on the fusion activity of the HIV-1 gp41 fusion domain as probed by lipid mixing. Qualitatively, the same result (i.e., positive fusion activity) was observed for the intact P-gp41$^{1-30}$-DYKDDDDK fusion domain construct used for the NMR studies (data not shown). In this case significant lipid mixing (∼30%) was observed on the time scale of 5−10 min (versus ∼2 min for the shorter gp41$^{1-23}$ peptides; Figure 2), most likely due to reduced solubility of the peptide under the assay conditions.

Oligomeric State and Conformation of the HIV-1 gp41 Fusion Domain in Different Detergents. The SDS:peptide ratio in the NMR samples was ca. 110. This translates to less than one fusion domain molecule per micelle, since the aggregation number of SDS (i.e., number of SDS molecules per micelle) is approximately 80 under the experimental conditions (*89*). Moreover, according to SDS−PAGE assays the fusion domain migrates as a single band with a molecular mass of ca. 4 kDa, corresponding to a monomeric peptide species (data not shown), and the peptide NMR spectrum was found to be independent of the SDS:peptide ratio over the range of ca. 80−500. Finally, ^{15}N spin relaxation parameters are consistent with the presence of a monomeric peptide species under the experimental conditions (see Discussion below).

A 600 MHz ^{1}H−^{15}N HSQC spectrum of the HIV-1 gp41 fusion domain in complex with an SDS micelle is shown in
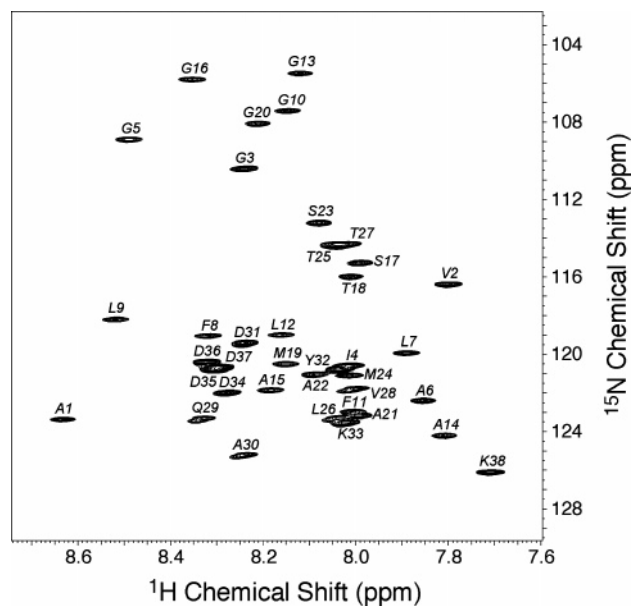
FIGURE 3: Two-dimensional 600 MHz $^{15}N-^1H$ HSQC spectrum of the HIV-1 gp41 fusion domain in complex with an SDS micelle. Sample conditions: 0.7 mM $^{15}N,^{13}C,^2H$-labeled HIV-1 gp41 fusion domain in 75 mM SDS at pH 6.5 (see Materials and Methods section for additional details). The spectrum was acquired using the sensitivity- and gradient-enhanced HSQC pulse scheme (*107*), as a 256* × 440* data matrix with acquisition times of 153 ms (t_1, ^{15}N) and 54 ms (t_2, ^1H), using four scans per FID and a total measurement time of 48 min. Resonance assignments are indicated (see Supporting Information, Table S1).

Figure 3. In this spectrum, acquired in less than 1 h (see Figure 3 legend for details), the signal-to-noise ratio for individual amide resonances corresponding to the fusion domain is greater than 100:1. Sequential backbone resonance assignments were obtained using a suite of 3D triple resonance experiments, which correlate the NMR frequencies of $^1H^\alpha$, $^1H^N$, ^{15}N, $^{13}C'$, $^{13}C^\alpha$, and $^{13}C^\beta$ nuclei (see Supporting Information, Figure S1, for representative spectra and Table S1 for resonance assignments). The $^1H^\alpha$, $^{13}C'$, $^{13}C^\alpha$, and $^{13}C^\beta$ secondary chemical shifts (see Supporting Information, Figure S2) indicate that residues Ile-4 to Ala-22 have conformations in the helical region of Ramachandran space, while the remaining residues, Ala-1 to Gly-3 and Ser-23 to Ala-30 of HIV-1 gp41 and the DYKDDDDK tag, exhibit random coil chemical shifts. Consequently, a TALOS database search (*87*) identifies mostly helical fragments for residues 4−22. This region also exhibits $^3J_{HNH\alpha}$ couplings, $H^N_i-H^N_{i+1}$, $H^\alpha_i-H^N_{i+1}$, and $H^\alpha_i-H^N_{i+3}$ NOEs (data not shown) (*59*), and RDC patterns (Figures 4 and 5) (*90*) characteristic of helical conformation.

Detailed characterization of the HIV-1 gp41 fusion domain (see Discussion below) was performed in negatively charged SDS micelles. As noted in the Materials and Methods section, the reason for the choice of this membrane mimetic was the optimal sample stability relative to other detergents. Note that our attempts to measure $^1H-^{15}N$ RDCs for the fusion domain reconstituted into DPC or LPPG micelles were unsuccessful (data not shown). This was due to the poor quality of the 2D $^1H-^{15}N$ IPAP-HSQC spectra recorded for the aligned sample, where the only detectable correlations corresponded to some of the most dynamically disordered residues of the fusion domain (residues 2−3 and 25−30) and the solubility enhancement tag. However, we were able
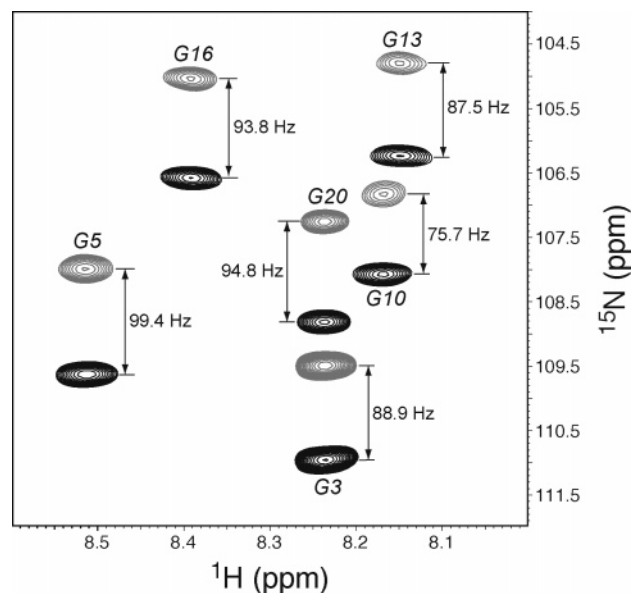
FIGURE 4: Small region of a two-dimensional 600 MHz $^{15}N-^1H$ IPAP-HSQC spectrum (*81*) of the HIV-1 gp41 fusion domain aligned using a stretched polyacrylamide gel (see Materials and Methods). The $J + D$ splittings (in Hz) are measured from the frequency differences observed in spectra obtained by taking the sum (black contours) and difference (gray contours) of the in-phase (IP) and antiphase (AP) HSQC spectra.
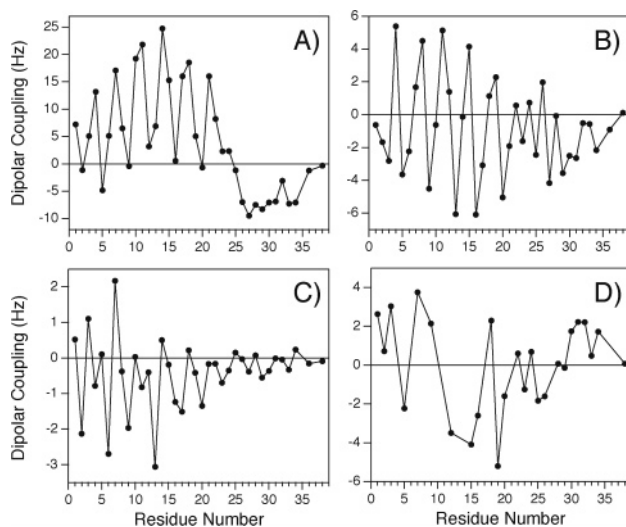
FIGURE 5: Residual dipolar couplings measured for the HIV-1 gp41 fusion domain plotted as a function of residue number. Shown are (A) $^{15}N-^1H$, (B) $^{13}C'-^{13}C^\alpha$, (C) $^{13}C'-^{15}N$, and (D) $^{13}C^\alpha-^{13}C^\beta$ couplings. The RDCs take into account the negative sign of the one-bond $^{15}N-^1H$ and $^{13}C'-^{15}N$ J-couplings. Note that residues are labeled according to $^{15}N-^1H$ correlations observed in 3D HNCO and HN(CO)CA experiments; i.e., $^{13}C'-^{13}C^\alpha$, $^{13}C'-^{15}N$, and $^{13}C^\alpha-^{13}C^\beta$ RDCs shown for residue i in plots B−D actually correspond to residue $i - 1$.

to record $^1H-^{15}N$ HSQC spectra in other detergents including DPC, mixed SDS/DPC, and LPPG micelles (see Supporting Information, Figure S3, for representative spectra). These data show that the majority of ^1H and ^{15}N chemical shifts, in particular those for the core residues (Ala-6 to Gly-20) of the fusion domain, are within 0.2 and 0.5 ppm, respectively, for spectra recorded in different detergents (see Figure S4). Furthermore, no increased line broadening is seen for resonances that exhibit the largest chemical shift changes. This excludes the presence of a dynamic equilibrium between

a monomeric and dimeric or trimeric species, which should lead to exchange broadening as the cause of the chemical shift changes. The similarity of the observed chemical shifts, which are very sensitive reporters of the local electronic environment, strongly indicates that the HIV-1 gp41 fusion domain adopts analogous structures in negatively charged and zwitterionic membrane mimetics (*91*). This observation is further supported by comparing our results with those obtained by Chou et al. (*51*) for a membrane-associated peptide corresponding to residues 282−304 of HIV-1 gp41 in DHPC micelles and isotropic ($q = 0.25$) DMPC/DHPC bicelles. In that study a relatively subtle change in the α-helical curvature of the peptide was associated with average absolute chemical shift changes, $|\Delta\delta|$, of ca. 0.1 ppm for $^1H^N$ and 0.6 ppm for ^{15}N, with $|\Delta\delta(^{15}N)| > 0.5$ ppm observed for 10 out of 22 residues. By comparison, average absolute chemical shift differences of ca. 0.1 ppm for $^1H^N$ and 0.3 ppm for ^{15}N are observed for the HIV-1 gp41 fusion domain (Figure S4), with only 3 of 22 ^{15}N shifts differing by more than 0.5 ppm for the most structured core residues (residues Gly-3 to Met-24).

Structure, *Dynamics*, *and Micelle Orientation of the HIV-1 Fusion Domain.* As noted above, the cursory examination of chemical shift, *J*-coupling, NOE, and RDC data indicates that residues Ile-4 to Ala-22 of the fusion domain adopt helical conformations, whereas the remaining residues exhibit coil-like spectral characteristics. These measurements, however, do not provide direct information about conformational dynamics or peptide orientation relative to the micelle. In this section we evaluate in detail the three-dimensional structure of the HIV-1 gp41 fusion domain in the micelle-bound state and establish links between peptide structure, dynamics, and membrane orientation.

Detailed characterization of peptide backbone dynamics is important twofold. First, increased mobility in certain regions of the molecule may have functional relevance, and second, conformational dynamics influence the measurement of geometric restraints and must be considered in the course of structure refinement. NMR techniques for characterization of fast (picosecond to nanosecond) time scale dynamics are well established and typically utilize spin relaxation properties of amide ^{15}N nuclei (R_1, R_2, and $\{^1H\}-^{15}N$ NOE) to probe backbone motions (*92*). In Figure 6, we show these parameters for the HIV-1 gp41 fusion domain as a function of residue number (see Supporting Information, Figure S6, for representative measurements). While ^{15}N longitudinal relaxation rates (R_1) are relatively constant for the fusion domain residues ($\langle R_1 \rangle = 1.57 \pm 0.06$ s^{-1}), transverse relaxation rates (R_2) span values differing by more than a factor of 3, and $\{^1H\}-^{15}N$ NOEs range from −0.3 to 0.7 with the highest R_2 and NOE values observed for residues 5−20. The ^{15}N spin relaxation data were analyzed using the model-free approach (*93*, *94*) to yield residue-specific generalized order parameters, S^2 (see Discussion below). An isotropic tumbling model was assumed, yielding an overall rotational correlation time of $\tau_c = 8.0$ ns for the micelle-bound HIV-1 gp41 fusion domain. A correlation time of this magnitude, characteristic of a ca. 15 kDa protein tumbling isotropically in solution, is consistent with a monomeric micelle-bound peptide and mirrors τ_c values in the 8−10 ns regime observed for a 5.5 kDa single transmembrane helix corresponding to the β subunit of *Rhodobacter sphaeroides*
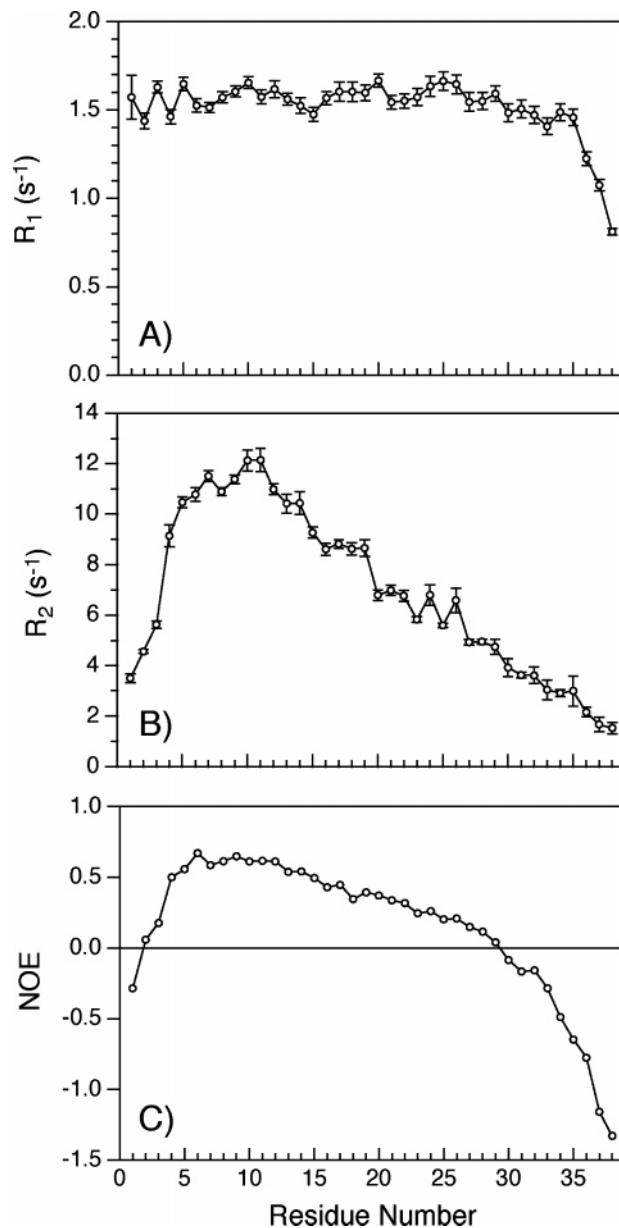
FIGURE 6: Relaxation parameters for the HIV-1 gp41 fusion domain. Shown are (A) ^{15}N R_1, (B) ^{15}N R_2, and (C) $\{^1H\}-^{15}N$ NOE values determined at 14.1 T as a function of residue number. Uncertainties in the $\{^1H\}-^{15}N$ NOE values are similar to the size of the plotted symbols and are not shown.

photosynthetic bacterial light harvesting 1 complex in different membrane mimetics (*91*). Since a peptide−micelle complex consisting of a single HIV-1 gp41 fusion domain and ∼70−80 SDS molecules corresponds to a molecular mass of ∼25 kDa, this τ_c is consistent with the observations of Girvin and co-workers (*91*), which indicate that protein−micelle complexes of this type may not necessarily tumble as single entities but rather that certain membrane mimetics are fluid enough to allow significant mobility of the peptide or protein within the confines of the micelle. Although in this work we have not rigorously measured the number of SDS molecules in the peptide−micelle complex, recent studies on at least one other system of this type, α-synuclein in SDS micelles, indicate that the number of SDS molecules in the protein−micelle complex approximates the aggregation number for free SDS (*56*, *95*).

Relaxation data for residues Ile-4 to Ala-15 were modeled using two parameters, the generalized order parameter, S^2, and the time constant for rapid internal motions, τ_e, in the 0−300 ps range (*93, 94*). Data for the remaining residues required a three-parameter model (*96*), which included S^2_f, S^2, and τ_e in the ∼0.5−1 ns regime to describe motions on fast and slow time scales. The resulting generalized order parameters (Figure 7A) reveal pronounced differences in the backbone dynamics within the micelle-associated fusion domain. Residues Ala-1 to Gly-3 exhibit enhanced picosecond to nanosecond time scale dynamics as indicated by relatively low order parameters (S^2 < 0.4). Starting with residue Ile-4, however, there is a sharp increase in S^2 to ca. 0.8 as the peptide backbone becomes less flexible; this increased rigidity (reflected in S^2 values in the 0.7−0.95 range) persists until residue Met-19. At this point of the sequence, the backbone becomes increasingly flexible, and in an approximately linear fashion S^2 decreases to almost zero toward the C-terminus.

Large differences in conformational dynamics in different regions of the fusion domain are also readily detected by the measurement of backbone RDCs (*97*). This can be demonstrated by using the molecular fragment replacement (MFR) method (*98*), where measured RDCs are best fit to a database of proteins of known structure for overlapping short peptide fragments along the sequence; MFR includes an independent optimization of the local alignment tensor parameters for each fragment. Figure 7B shows a plot of the MFR-derived generalized molecular alignment tensor magnitude (*99*) as a function of residue number. A nearly 2-fold decrease in the alignment tensor magnitude is observed for the C-terminal residues relative to the N-terminal residues, which is consistent with the enhanced picosecond to nanosecond time scale dynamics derived from ^{15}N relaxation data (cf. Figure 7A). In addition, we note that the MFR search yields only extended conformations for the dynamically disordered C-terminal residues, in agreement with the notion of Annila and co-workers (*100*) that elongated conformations are emphasized when measuring RDCs for molecules undergoing substantial internal motion. Similar effects of backbone dynamics on the magnitude of the local alignment tensor were also observed in a recent study of micelle-bound α-synuclein (*56*). The practical significance of these results is that the variable backbone dynamics of the fusion domain must be carefully considered during high-resolution structure refinement. In the current work this was accomplished as follows: during the refinement protocol RDC restraints were included only for the least mobile residues, Ile-4 to Met-19, which exhibited generalized order parameters of S^2 > 0.65, and the RDCs within this region were scaled by a factor of $(S^2)^{-1/2}$ in a residue-specific fashion. This scaling of RDCs, to first order, compensates for the effect of internal dynamics when defining the time-averaged orientation of the corresponding vectors (*75*).

The increased conformational dynamics near the C-terminus are also correlated with the positioning of the fusion domain in the micelle, which was probed qualitatively by measuring the exchange of amide protons with the solvent in site-specific fashion. The data in Figure 7C show that residues with the highest order parameters (Ile-4 to Ala-15) exhibit minimal exchange with the solvent at different pH values. This implies that these residues are involved in stable
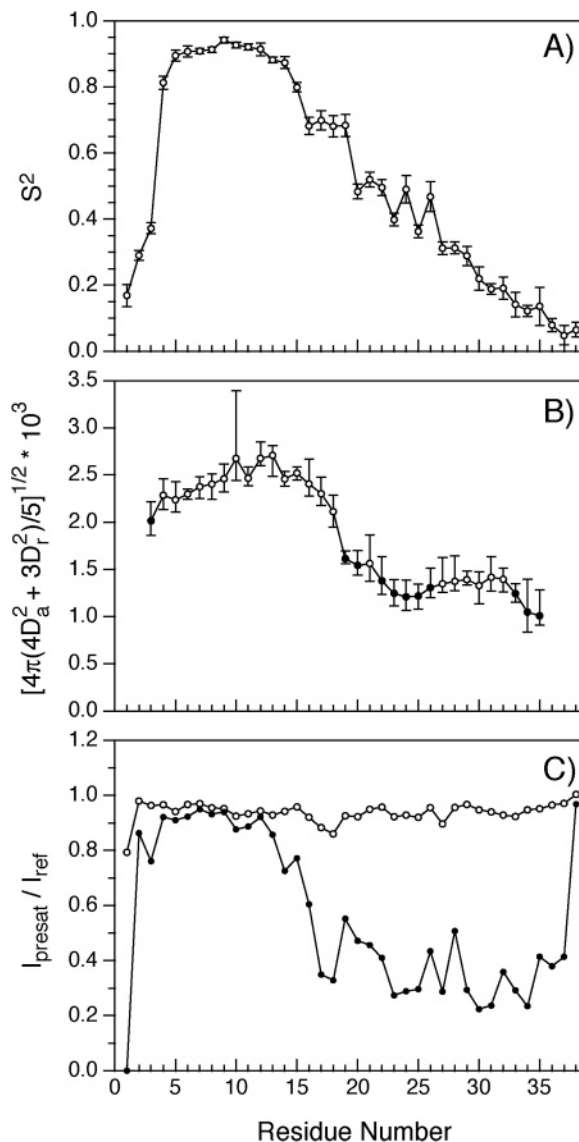
FIGURE 7: (A) Generalized order parameters, S^2, obtained from the analysis of amide backbone ^{15}N relaxation data (cf. Figure 6) using the program Modelfree 4.15 (*108, 109*). An isotropic model was used to fit the data, yielding an overall rotational correlation time of τ_c = 8.0 ns for the HIV-1 gp41 fusion domain. ^{15}N relaxation data for residues 4−15 could be successfully modeled using two parameters (*93*), S^2 and τ_e, in the 0−300 ps range, whereas a three-parameter model (*96*), which included S^2_f, S^2, and τ_e in the ∼0.5−1 ns regime, was used to fit the data for residues 1−3 and 16−38. (B) Generalized alignment tensor magnitudes (*99*), $[4\pi(4D_a^2 + 3D_r^2)/5]^{1/2}$, derived from a molecular fragment replacement (MFR) procedure (*98*), including their range among the 10 best fitting database fragments. During MFR, the measured RDCs are compared to a database of dipolar coupling values expected for overlapping fragments of seven residues along the sequence. The residue number in the plot corresponds to the central residue for each fragment; i.e., no predictions are available for the three N- and C-terminal residues. Solid symbols indicate those residues for which MFR did not yield a unique cluster of ϕ/ψ angles irrespective of the position of the residue within the fragment. (C) Qualitative investigation of the exchange of amide protons with the solvent. Shown are ratios of peak intensities in 2D ^{15}N−^{1}H HSQC spectra of the HIV-1 gp41 fusion domain recorded at pH 5.8 (○) and pH 7.2 (●) in the absence and presence of a selective water presaturation pulse during the 1.5 s relaxation delay between scans (*86*). Note that a value of zero has been assigned to the I_{presat}/I_{ref} ratio for Ala-1 at pH 7.2, because no intensity is observed in the reference spectrum recorded at this pH, due to very rapid exchange with the solvent.
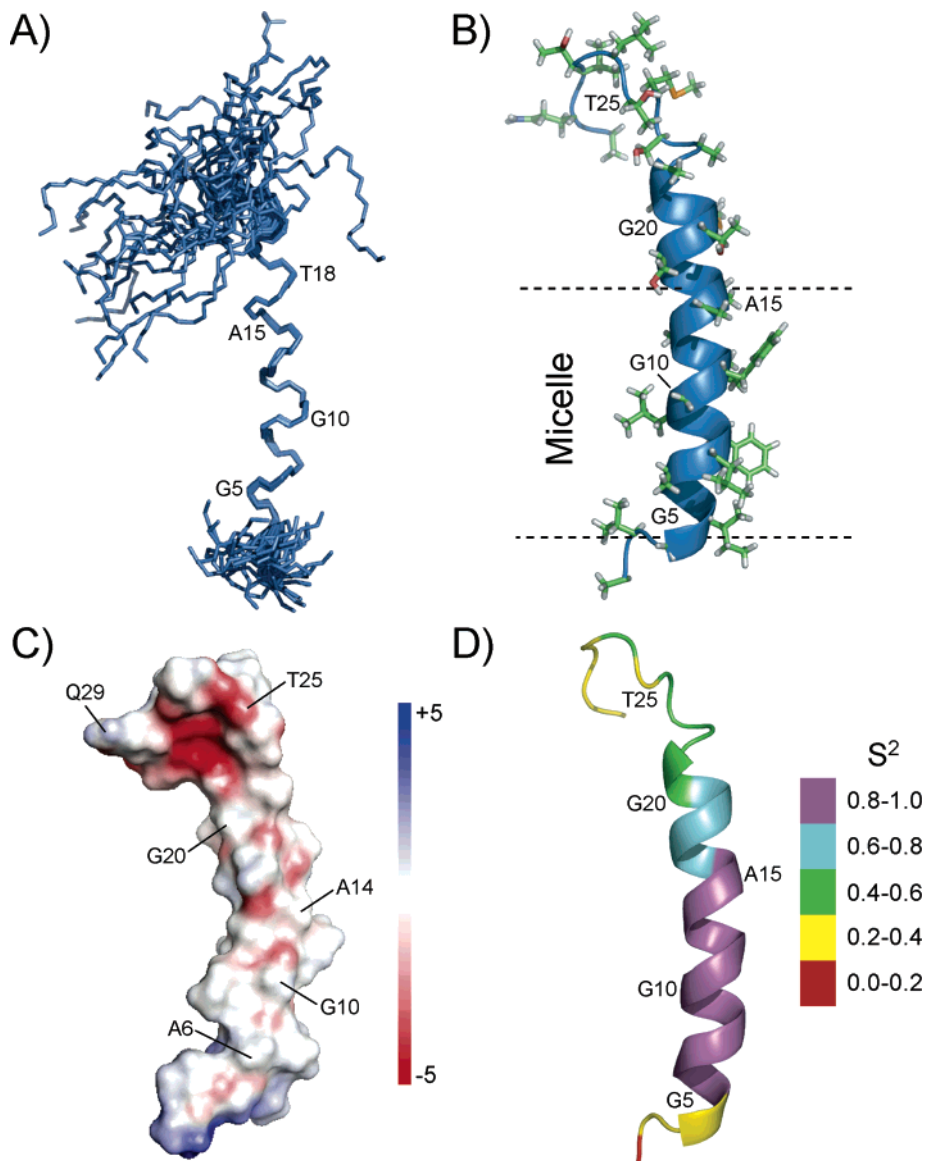
FIGURE 8: (A) Ensemble of 30 structures of the HIV-1 gp41 fusion domain in an SDS micelle. The structures are superimposed over the backbone N, C$^\alpha$, and C′ atoms (coordinate rmsd 0.13 Å) of the least mobile residues, Ile-4 to Met-19. (B) Ribbon representation of the HIV-1 gp41 fusion domain structure. The "typical" conformer shown exhibits the best agreement between the observed and fitted RDCs. Side chains are included for reference, but note that due to χ^1 rotamer averaging no experimental side-chain dihedral restraints were included in the refinement. The approximate location of the peptide with respect to the micelle (with residues Gly-3 and Gly-16 found at the micelle−solvent interfaces), based on measurements of the exchange of amide protons with the solvent and NOE interactions between H^N resonances of Ile-4 to Ala-15 and those of the detergent alkyl chain, is also indicated. (C) Electrostatic surface potential (ϕ) representation of the HIV-1 gp41 fusion domain structure, generated using the program APBS (*110*). Negative (−5 kT/e < ϕ < 0 kT/e), positive (0 kT/e < ϕ < 5 kT/e), and neutral potentials are shown in red, blue, and white, respectively. (D) Backbone dynamics mapped onto the structure of the HIV-1 gp41 fusion domain. Residues are colored according to the generalized order parameters, S^2, obtained from the analysis of amide backbone ^{15}N relaxation data (cf. Figures 6 and 7A) as follows: magenta ($0.8 \le S^2 < 1$), cyan ($0.6 \le S^2 < 0.8$), green ($0.4 \le S^2 < 0.6$), yellow ($0.2 \le S^2 < 0.4$), and red ($0 \le S^2 < 0.2$). The figure was prepared using the program PyMOL (*111*).

hydrogen bonds, are inaccessible to solvent, and span the length of the micelle, while the ca. two to three N-terminal residues and residues Gly-16 to Ala-30 protrude into the solvent. Embedding of this region in the micelle is supported by a continuous set of NOE interactions between the amide H^N resonances of Ile-4 to Ala-15 and those of the detergent alkyl chain (data not shown). Our findings are consistent with the location of the HIV-1 gp41 fusion domain within the micelle, as deduced from broadening of NMR resonances in the presence of spin-labeled detergent molecules (*35*).

In Figure 8 we summarize the three-dimensional structure of the micelle-bound HIV-1 gp41 fusion domain, determined using solution-state NMR methods. As noted above, residues

Ile-4 to Ala-22 adopt helical conformations, while the remaining residues are dynamically disordered. In particular, a well-defined, uninterrupted α-helix is observed for residues Ile-4 to Met-19 as evidenced by the small spread in the backbone torsion angles for the ensemble of 30 fusion domain structures shown in Figure 8A (see Table 1 for the summary of structural statistics). No explicit side-chain restraints were used in the structure calculations since $^3J_{NC\gamma}$ and $^3J_{C'C\gamma}$ coupling measurements indicate that rapid χ^1 rotamer averaging takes place for the vast majority of residues (see, e.g., Supporting Information, Figure S5). The relatively low coordinate rmsd for the backbone atoms of Ile-4 to Met-19 is mainly the result of the large number of

Table 1: Structural Statistics for the HIV-1 gp41 Fusion Domain

experimental NMR restraints	
total restraints[a]	192
dipolar coupling restraints	57
dihedral restraints	38
NOE distance restraints	74
J-coupling restraints	23
rms deviation from experimental restraints	
N−H dipolar couplings (Hz)	1.27 ± 0.10
N−C′ dipolar couplings (Hz)	0.27 ± 0.02
C′−C$^\alpha$ dipolar couplings (Hz)	0.78 ± 0.01
C$^\alpha$−C$^\beta$ dipolar couplings (Hz)	0.62 ± 0.03
dihedral angles (deg)	0.1 ± 0.2
NOEs (Å)	0.22 ± 0.04
J-couplings (Hz)	0.97 ± 0.02
deviations from idealized covalent geometry	
bonds (Å)	0.0033 ± 0.0002
angles (deg)	0.55 ± 0.02
impropers (deg)	0.46 ± 0.01
energy (kcal mol^{-1})	
total	214 ± 12
bond	5.9 ± 0.7
angle	44 ± 3
improper	8.5 ± 0.5
van der Waals	15 ± 2
dipolar	89 ± 2
dihedral	0.1 ± 0.1
NOE	18 ± 7
J-coupling	33 ± 2
atomic rms deviations (Å)[b]	
backbone	0.13
all heavy atom	0.95
Ramachandran statistics[c]	
ϕ/ψ in most favored regions (%)	97.0
ϕ/ψ in additionally allowed regions (%)	3.0

[a] Dipolar coupling restraints (16 N−H, 16 N−C′, 16 C′−C$^\alpha$, 9 C$^\alpha$−C$^\beta$) were included for the least mobile residues I4−M19 ($S^2 > 0.65$) and scaled by a factor of $(S^2)^{-1/2}$ in a residue-specific fashion. Dihedral restraints (19 ϕ, 19 ψ) were derived from TALOS (87) for residues I4−A22. NOE restraints involving H^N for residues V2−M24 were of the following types: 18 H^N_i−H$^N_{i+1}$, 25 H$^\alpha_i$−H$^N_{i+1}$, 13 H$^\beta_i$−H$^N_{i+1}$, 2 H^N_i−H$^N_{i+2}$, 5 H$^\alpha_i$−H$^N_{i+2}$, and 11 H$^\alpha_i$−H$^N_{i+3}$. J-coupling ($^3J_{HNH\alpha}$) restraints were included for residues V2−M24. [b] As evaluated with the program MOLMOL (105) for residues I4−M19, for which RDC restraints were used in the structure refinement. Atomic rms deviations for residues I4−A22 are 0.46 Å (backbone) and 1.03 Å (all heavy atom). [c] As evaluated with the program PROCHECK (106) for residues I4−A22.

RDC restraints used for deriving this structure (three to four RDCs per residue) and only reflects the precision at which the average structure is determined, not the amplitude of structural fluctuations. As demonstrated by previous studies (51), RDC restraints are uniquely suited for characterizing global features about the structure, typically not accessible from NOEs and J-couplings in nonglobular molecules such as membrane-associated peptides and nucleic acids. In Figure 8B−D, links between the three-dimensional fusion domain structure and other peptide properties are established. Figure 8B shows a ribbon representation of a typical conformer from the ensemble of calculated structures and indicates the section of the fusion domain embedded in the micelle. The burial of peptide residues within the micelle is highly correlated with the backbone dynamics, where the generalized order parameters, mapped onto the fusion domain structure in Figure 8D, reveal a gradual increase in the peptide backbone mobility for extramicellar residues. Finally, in Figure 8C an electrostatic surface potential representation of the fusion domain structure is shown. As expected, the surface of the

fusion domain is highly hydrophobic particularly for the micelle-embedded portion.

DISCUSSION

The ultimate goal of research on membrane fusion domains is to gain as much insight as possible about their role in promoting virus−cell fusion. A vast amount of work on fusion peptides, employing a variety of spectroscopic and computational methods (20−22, 32−45), has revealed that the detailed characterization of these systems in terms of a single fusion-active conformation poses a significant challenge. Fusion peptides appear to exhibit a high degree of conformational flexibility, presumably aiding them to switch their secondary structure depending on factors such as the peptide to lipid ratio, lipid composition, and presence of cholesterol in the membrane mimetic (20−22, 32−45). Specifically, it has been found that lower peptide to lipid ratios (20−22) and the absence of cholesterol in the membrane mimetic (44) typically favor monomeric helical fusion peptide conformations, whereas oligomeric β-strand conformations are found at high peptide to lipid ratios and in the presence of cholesterol. Although the observed effect of peptide to lipid ratio on the peptide's aggregation state and associated secondary structure appears reasonable, the questions of precisely how and why cholesterol influences the fusion peptide conformation are still open. Indeed, while high cholesterol concentration in the HIV-1 membrane is crucial to viral fusion and infectivity (101, 102), a recent study has shown that cholesterol depletion in the host cell affects the association of the gp120/gp41 complex with the cellular receptors but not the fusion event itself (103). Moreover, a recent study by Weliky and co-workers (43) notes that positive fusion activity was obtained for the HIV-1 fusion domain in lipid mixing assays under conditions where the fusion peptide adopts either helical or β-strand conformations. In light of the large amount of sometimes apparently contradictory data on fusion domains, we believe that detailed studies of these systems under a variety of experimental conditions are warranted and important for gaining a more detailed insight into the structural basis of the membrane fusion process. Consequently, the main goal of the current work is the characterization of the three-dimensional structure and molecular dynamics of the HIV-1 gp41 fusion domain, in a well-defined membrane-mimicking environment provided by detergent micelles at a relatively low peptide to lipid ratio.

While the data presented here corroborate in part the conclusions of several previous solution-state NMR studies of micelle-bound HIV-1 gp41 fusion domains (35, 42), they provide new insights about the three-dimensional structure and backbone and side-chain dynamics of this system that have not been discussed in detail previously and can be related to the mechanism of viral membrane fusion. First, we firmly establish that residues Ile-4 to Met-19 of the fusion domain form a nearly ideal α-helix (residues Gly-20 to Ala-22 are also found to adopt helical conformations), which spans the micelle and protrudes into the solvent. This conclusion, based primarily on the measurement of an extensive set of backbone RDCs, rules out the presence of a type I β-turn between Ser-17 and Gly-20 and any significant interactions of residues Gly-20 to Ser-23 with the micelle surface as suggested by the study of a 23-residue

fusion peptide from the LAV$_{1a}$ strain of HIV-1 gp41 by Chang et al. (*35*). It is possible that this discrepancy results from our use of a longer peptide construct relative to the 23-residue peptide used in the previous study (*35*). However, our results in SDS micelles are also consistent with the general conclusions of Morris et al. (*42*), who investigated the same 23-residue fusion peptide in complex with zwitterionic DPC micelles using ^{1}H NMR techniques and also found no evidence of the type I β-turn. Combined with the results of our measurements in LPPG and DPC micelles, this strongly suggests that the three-dimensional structure of the HIV-1 gp41 fusion domain is largely independent of the exact structure and charge of the lipid headgroups and is governed primarily by the amino acid sequence of the fusion domain and/or presence of other molecules, such as cholesterol, in the lipid bilayer. Second, we find that rapid χ^1 rotamer averaging takes place for the vast majority of residues (see, e.g., Supporting Information, Figure S5). Such presence of χ^1 rotamer averaging appears to be reasonable for the HIV-1 gp41 fusion domain under the experimental conditions employed here; the peptide is a monomer in the micelle-bound state, and only limited conformational restraints are imposed on the side chains by each other or by the peptide backbone. Third, the data presented here reveal that fusion domain residues Ser-23 to Ala-30 adopt coil-like conformations and exhibit enhanced picosecond to nanosecond time scale backbone dynamics. These features of the HIV-1 gp41 fusion domain, not explored in detail by previous studies, are likely to be significant in the context of membrane fusion. In particular, they provide a possible explanation of how the membrane-interacting portion of HIV-1 gp41 interacts with the stable α-helical ectodomain (*8−10*), namely, via a flexible linker of 8−10 residues.

The detailed characterization of the peptide backbone structure and dynamics in the micelle-bound state allows us to speculate further about the potential formation of fusion domain oligomers in the fusion-active state of HIV-1. Given the trimeric nature of the intact gp120/gp41 complex (*8−10*), it is feasible and likely that, for the helical conformation of the fusion domain discussed here, the individual α-helices assemble into trimers. If a higher order structure of this type is indeed formed, the individual helices are expected to retain the majority of the features of the monomer backbone structure, and the oligomerization is expected to be mediated by side-chain to side-chain interactions, in which case the side chains in the core region of the fusion peptide would adopt well-defined rotameric states as they do in the interior of folded globular proteins (in contrast to the rotamer-averaged conformations observed for the monomeric fusion domain). The assumption that minimal changes in the monomer backbone structure are required for the formation of a fusion domain trimer is supported by the recent study of glycophorin A by Fisher et al. (*104*), who have shown that oligomerization had no significant impact on the secondary structure of the glycophorin A helix.

In summary, we have used multidimensional solution-state NMR techniques to investigate in detail the three-dimensional structure and dynamics of the micelle-bound HIV-1 gp41 fusion domain. Residual dipolar couplings recorded for the fusion domain−micelle complex, aligned with respect to the magnetic field, were especially critical in revealing details of the structure (and dynamics) typically not accessible from NOEs and *J*-couplings. Moreover, detailed characterization of the backbone dynamics from ^{15}N spin relaxation measurements enabled links to be established between the fusion domain structure, dynamics, and position in a detergent micelle, all directly related to development of a better understanding of the mechanism of HIV-1 viral membrane fusion.

ACKNOWLEDGMENT

SUPPORTING INFORMATION AVAILABLE

Six figures and one table as described in the text. This material is available free of charge via the Internet at http://pubs.acs.org.

REFERENCES

1. Hernandez, L. D., Hoffman, L. R., Wolfsberg, T. G., and White, J. M. (1996) Virus-cell and cell-cell fusion, *Annu. Rev. Cell Dev. Biol. 12*, 627−661.
2. Weissenhorn, W., Dessen, A., Calder, L. J., Harrison, S. C., Skehel, J. J., and Wiley, D. C. (1999) Structural basis for membrane fusion by enveloped viruses, *Mol. Membr. Biol. 16*, 3−9.
3. Eckert, D. M., and Kim, P. S. (2001) Mechanisms of viral membrane fusion and its inhibition, *Annu. Rev. Biochem. 70*, 777−810.
4. Blumenthal, R., Clague, M. J., Durell, S. R., and Epand, R. M. (2003) Membrane fusion, *Chem. Rev. 103*, 53−69.
5. Jahn, R., Lang, T., and Sudhof, T. C. (2003) Membrane fusion, *Cell 112*, 519−533.
6. Bullough, P. A., Hughson, F. M., Skehel, J. J., and Wiley, D. C. (1994) Structure of influenza haemagglutinin at the pH of membrane fusion, *Nature 371*, 37−43.
7. Fass, D., Harrison, S. C., and Kim, P. S. (1996) Retrovirus envelope domain at 1.7 Å resolution, *Nat. Struct. Biol. 3*, 465−469.
8. Weissenhorn, W., Dessen, A., Harrison, S. C., Skehel, J. J., and Wiley, D. C. (1997) Atomic structure of the ectodomain from HIV-1 gp41, *Nature 387*, 426−430.
9. Chan, D. C., Fass, D., Berger, J. M., and Kim, P. S. (1997) Core structure of gp41 from the HIV envelope glycoprotein, *Cell 89*, 263−273.
10. Tan, K., Liu, J.-H., Wang, J.-H., Shen, S., and Lu, M. (1997) Atomic structure of a thermostable subdomain of HIV-1 gp41, *Proc. Natl. Acad. Sci. U.S.A. 94*, 12303−12308.
11. Caffrey, M., Cai, M., Kaufman, J., Stahl, S. J., Wingfield, P. T., Covell, D. G., Gronenborn, A. M., and Clore, G. M. (1998) Three-dimensional solution structure of the 44 kDa ectodomain of SIV gp41, *EMBO J. 17*, 4572−4584.
12. Malashkevich, V. N., Chan, D. C., Chutkowski, C. T., and Kim, P. S. (1998) Crystal structure of the simian immunodeficiency virus (SIV) gp41 core: conserved helical interactions underlie the broad inhibitory activity of gp41 peptides, *Proc. Natl. Acad. Sci. U.S.A. 95*, 9134−9139.
13. Yang, Z. N., Mueser, T. C., Kaufman, J., Stahl, S. J., Wingfield, P. T., and Hyde, C. C. (1999) The crystal structure of the SIV gp41 ectodomain at 1.47 Å resolution, *J. Struct. Biol. 126*, 131−144.
14. Baker, K. A., Dutch, R. E., Lamb, R. A., and Jardetzky, T. S. (1999) Structural basis for paramyxovirus-mediated membrane fusion, *Mol. Cell 3*, 309−319.
15. Weissenhorn, W., Carfi, A., Lee, K. H., Skehel, J. J., and Wiley, D. C. (1998) Crystal structure of the Ebola virus membrane fusion subunit, GP2, from the envelope glycoprotein ectodomain, *Mol. Cell 2*, 605−616.

16. Malashkevich, V. N., Schneider, B. J., McNally, M. L., Milhollen, M. A., Pang, J. X., and Kim, P. S. (1999) Core structure of the envelope glycoprotein GP2 from Ebola virus at 1.9-Å resolution, *Proc. Natl. Acad. Sci. U.S.A. 96*, 2662−2667.

17. Kwong, P. D., Wyatt, R., Robinson, J., Sweet, R. W., Sodroski, J., and Hendrickson, W. A. (1998) Structure of an HIV gp120 envelope glycoprotein in complex with the CD4 receptor and a neutralizing human antibody, *Nature 393*, 648−659.

18. Berger, E. A., Murphy, P. M., and Farber, J. M. (1999) Chemokine receptors as HIV-1 coreceptors: Roles in viral entry, tropism, and disease, *Annu. Rev. Immunol. 17*, 657−700.

19. Weissenhorn, W., Calder, L. J., Dessen, A., Laue, T., Skehel, J. J., and Wiley, D. C. (1997) Assembly of a rod-shaped chimera of a trimeric GCN4 zipper and the HIV-1 gp41 ectodomain expressed in *Escherichia coli*, *Proc. Natl. Acad. Sci. U.S.A. 94*, 6065−6069.

20. Durell, S. R., Martin, I., Ruysschaert, J. M., Shai, Y., and Blumenthal, R. (1997) What studies of fusion peptides tell us about viral envelope glycoprotein-mediated membrane fusion, *Mol. Membr. Biol. 14*, 97−112.

21. Nieva, J. L., and Agirre, A. (2003) Are fusion peptides a good model to study viral cell fusion?, *Biochim. Biophys. Acta 1614*, 104−115.

22. Epand, R. M. (2003) Fusion peptides and the mechanism of viral fusion, *Biochim. Biophys. Acta 1614*, 116−121.

23. Tamm, L. K., Han, X., Li, Y. L., and Lai, A. L. (2002) Structure and function of membrane fusion peptides, *Biopolymers 66*, 249−260.

24. Gething, M. J., Doms, R. W., York, D., and White, J. (1986) Studies of the mechanism of membrane fusion−Site specific mutagenesis of the hemagglutinin of influenza virus, *J. Cell Biol. 102*, 11−23.

25. Schoch, C., and Blumenthal, R. (1993) Role of the fusion peptide sequence in initial stages of influenza hemagglutinin-induced cell-fusion, *J. Biol. Chem. 268*, 9267−9274.

26. Steinhauer, D. A., Wharton, S. A., Skehel, J. J., and Wiley, D. C. (1995) Studies of membrane fusion activities of fusion peptide mutants of influenza hemagglutinin, *J. Virol. 69*, 6643−6651.

27. Qiao, H., Armstrong, R. T., Melikyan, G. B., Cohen, F. S., and White, J. M. (1999) A specific point mutant at position 1 of the influenza hemagglutinin fusion peptide displays a hemifusion phenotype, *Mol. Biol. Cell 10*, 2759−2769.

28. Delahunty, M. D., Rhee, I., Freed, E. O., and Bonifacino, J. S. (1996) Mutational analysis of the fusion peptide of the human immunodeficiency virus type 1: Identification of critical glycine residues, *Virology 218*, 94−102.

29. Pritsker, M., Rucker, J., Hoffman, T. L., Doms, R. W., and Shai, Y. (1999) Effect of nonpolar substitutions of the conserved Phe-11 in the fusion peptide of HIV-1 gp41 on its function, structure, and organization in membranes, *Biochemistry 38*, 11359−11371.

30. Lear, J. D., and DeGrado, W. F. (1987) Membrane binding and conformational properties of peptides representing the NH2 terminus of influenza HA-2, *J. Biol. Chem. 262*, 6500−6505.

31. Wharton, S. A., Martin, S. R., Ruigrok, R. W. H., Skehel, J. J., and Wiley, D. C. (1988) Membrane fusion by peptide analogues of influenza virus haemagglutinin, *J. Gen. Virol. 69*, 1847−1857.

32. Rafalski, M., Lear, J. D., and DeGrado, W. F. (1990) Phospholipid interactions of synthetic peptides representing the N-terminus of HIV gp41, *Biochemistry 29*, 7917−7922.

33. Nieva, J. L., Nir, S., Muga, A., Goni, F. M., and Wilschut, J. (1994) Interaction of the HIV-1 fusion peptide with phospholipid vesicles: Different structural requirements for fusion and leakage, *Biochemistry 33*, 3201−3209.

34. Martin, I., Schaal, H., Scheid, A., and Ruysschaert, J. M. (1996) Lipid membrane fusion induced by the human immunodeficiency virus type 1 gp41: N-terminal extremity is determined by its orientation in the lipid bilayer, *J. Virol. 70*, 298−304.

35. Chang, D. K., Cheng, S. F., and Chien, W. J. (1997) The amino-terminal fusion domain peptide of human immunodeficiency virus type 1 gp41 inserts into the sodium dodecyl sulfate micelle primarily as helix with a conserved glycine at the micelle-water interface, *J. Virol. 71*, 6593−6602.

36. Curtain, C., Separovic, F., Nielsen, K., Craik, D., Zhong, Y., and Kirkpatrick, A. (1999) The interactions of the N-terminal fusogenic peptide of HIV-1 gp41 with neutral phospholipids, *Eur. Biophys. J. 28*, 427−436.

37. Gordon, L. M., Mobley, P. W., Pilpa, R., Sherman, M. A., and Waring, A. J. (2002) Conformational mapping of the N-terminal peptide of HIV-1 gp41 in membrane environments using C-13-enhanced Fourier transform infrared spectroscopy, *Biochim. Biophys. Acta 1559*, 96−120.

38. Yang, J., Gabrys, C. M., and Weliky, D. P. (2001) Solid-state nuclear magnetic resonance evidence for an extended β strand conformation of the membrane-bound HIV-1 fusion peptide, *Biochemistry 40*, 8126−8137.

39. Han, X., and Tamm, L. K. (2000) A host-guest system to study structure-function relationships of membrane fusion peptides, *Proc. Natl. Acad. Sci. U.S.A. 97*, 13097−13102.

40. Han, X., Bushweller, J. H., Cafiso, D. S., and Tamm, L. K. (2001) Membrane structure and fusion-triggering conformational change of the fusion domain from influenza hemagglutinin, *Nat. Struct. Biol. 8*, 715−720.

41. Kamath, S., and Wong, T. C. (2002) Membrane structure of the human immunodeficiency virus gp41 fusion domain by molecular dynamics simulation, *Biophys. J. 83*, 135−143.

42. Morris, K. F., Gao, X. F., and Wong, T. C. (2004) The interactions of the HIV gp41 fusion peptides with zwitterionic membrane mimics determined by NMR spectroscopy, *Biochim. Biophys. Acta 1667*, 67−81.

43. Yang, J., Prorok, M., Castellino, F. J., and Weliky, D. P. (2004) Oligomeric β-structure of the membrane-bound HIV-1 fusion peptide formed from soluble monomers, *Biophys. J. 87*, 1951−1963.

44. Wasniewski, C. M., Parkanzky, P. D., Bodner, M. L., and Weliky, D. P. (2004) Solid-state nuclear magnetic resonance studies of HIV and influenza fusion peptide orientations in membrane bilayers using stacked glass plate samples, *Chem. Phys. Lipids 132*, 89−100.

45. Sackett, K., and Shai, Y. (2005) The HIV fusion peptide adopts intermolecular parallel β-sheet structure in membranes when stabilized by the adjacent N-terminal heptad repeat: A ^{13}C FTIR study, *J. Mol. Biol. 350*, 790−805.

46. MacKenzie, K. R., Prestegard, J. H., and Engelman, D. M. (1997) A transmembrane helix dimer: Structure and implications, *Science 276*, 131−133.

47. Rastogi, V. K., and Girvin, M. E. (1999) Structural changes linked to proton translocation by subunit c of the ATP synthase, *Nature 402*, 263−268.

48. Poulsen, S. A., Watson, A. A., Fairlie, D. P., and Craik, D. J. (2000) Solution structures in aqueous SDS micelles of two amyloid beta peptides of A beta(1−28) mutated at the alpha-secretase cleavage site (K16E, K16F), *J. Struct. Biol. 130*, 142−152.

49. Schibli, D. J., Montelaro, R. C., and Vogel, H. J. (2001) The membrane-proximal tryptophan-rich region of the HIV glycoprotein, gp41, forms a well-defined helix in dodecylphosphocholine micelles, *Biochemistry 40*, 9570−9578.

50. Arora, A., Abildgaard, F., Bushweller, J., and Tamm, L. K. (2001) Structure of outer membrane protein A transmembrane domain by NMR spectroscopy, *Nat. Struct. Biol. 8*, 334−338.

51. Chou, J. J., Kaufman, J. D., Stahl, S. J., Wingfield, P. T., and Bax, A. (2002) Micelle-induced curvature in a water-insoluble HIV-1 Env peptide revealed by NMR dipolar coupling measurement in stretched polyacrylamide gel, *J. Am. Chem. Soc. 124*, 2450−2451.

52. Mascioni, A., Karim, C., Barany, G., Thomas, D. D., and Veglia, G. (2002) Structure and orientation of sarcolipin in lipid environments, *Biochemistry 41*, 475−482.

53. Hwang, P. M., Choy, W. Y., Lo, E. I., Chen, L., Forman-Kay, J. D., Raetz, C. R. H., Prive, G. G., Bishop, R. E., and Kay, L. E. (2002) Solution structure and dynamics of the outer membrane enzyme PagP by NMR, *Proc. Natl. Acad. Sci. U.S.A. 99*, 13560−13565.

54. Park, S. H., Mrse, A. A., Nevzorov, A. A., Mesleh, M. F., Oblatt-Montal, M., Montal, M., and Opella, S. J. (2003) Three-dimensional structure of the channel-forming trans-membrane domain of virus protein "u" (Vpu) from HIV-1, *J. Mol. Biol. 333*, 409−424.

55. Fernandez, C., Hilty, C., Wider, G., Guntert, P., and Wuthrich, K. (2004) NMR structure of the integral membrane protein OmpX, *J. Mol. Biol. 336*, 1211−1221.

56. Ulmer, T. S., Bax, A., Cole, N. B., and Nussbaum, R. L. (2005) Structure and dynamics of micelle-bound human α-synuclein, *J. Biol. Chem. 280*, 9595−9603.

57. Tian, C. L., Breyer, R. M., Kim, H. J., Karra, M. D., Friedman, D. B., Karpay, A., and Sanders, C. R. (2005) Solution NMR spectroscopy of the human vasopressin V2 receptor, a G protein-coupled receptor, *J. Am. Chem. Soc. 127*, 8010−8011.

58. Oxenoid, K., and Chou, J. J. (2005) The structure of phospho-lamban pentamer reveals a channel-like architecture in membranes, *Proc. Natl. Acad. Sci. U.S.A. 102*, 10870−10875.

59. Wüthrich, K. (1986) *NMR of Proteins and Nucleic Acids*, Wiley, New York.

60. Bax, A., Kontaxis, G., and Tjandra, N. (2001) Dipolar couplings in macromolecular structure determination, *Methods Enzymol. 339*, 127−174.

61. Prestegard, J. H., Al-Hashimi, H. M., and Tolman, J. R. (2000) NMR structures of biomolecules using field oriented media and residual dipolar couplings, *Q. Rev. Biophys. 33*, 371−424.

62. Tycko, R., Blanco, F. J., and Ishii, Y. (2000) Alignment of biopolymers in strained gels: A new way to create detectable dipole-dipole couplings in high-resolution biomolecular NMR, *J. Am. Chem. Soc. 122*, 9340−9341.

63. Sass, H. J., Musco, G., Stahl, S. J., Wingfield, P. T., and Grzesiek, S. (2000) Solution NMR of proteins within polyacrylamide gels: Diffusional properties and residual alignment by mechanical stress or embedding of oriented purple membranes, *J. Biomol. NMR 18*, 303−309.

64. Chou, J. J., Gaemers, S., Howder, B., Louis, J. M., and Bax, A. (2001) A simple apparatus for generating stretched polyacrylamide gels, yielding uniform alignment of proteins and detergent micelles, *J. Biomol. NMR 21*, 377−382.

65. Hu, J. S., Grzesiek, S., and Bax, A. (1997) Two-dimensional NMR methods for determining χ¹ angles of aromatic residues in proteins from three-bond $J_{C'Cγ}$ and $J_{NCγ}$ couplings, *J. Am. Chem. Soc. 119*, 1803−1804.

66. Hu, J. S., and Bax, A. (1997) χ¹ angle information from a simple two-dimensional NMR experiment that identifies trans $^3J_{NCγ}$ couplings in isotopically enriched proteins, *J. Biomol. NMR 9*, 323−328.

67. Hope, M. J., Bally, M. B., Webb, G., and Cullis, P. R. (1985) Production of large unilamellar vesicles by a rapid extrusion procedure: Characterization of size distribution, trapped volume and ability to maintain a membrane potential, *Biochim. Biophys. Acta 812*, 55−65.

68. Struck, D. K., Hoekstra, D., and Pagano, R. E. (1981) Use of resonance energy transfer to monitor membrane fusion, *Biochemistry 20*, 4093−4099.

69. Piszkiewicz, D., Landon, M., and Smith, E. L. (1970) Anomalous cleavage of aspartyl-proline peptide bonds during amino acid sequence determinations, *Biochem. Biophys. Res. Commun. 40*, 1173−1178.

70. Hopp, T. P., Prickett, K. S., Price, V. L., Libby, R. T., March, C. J., Cerretti, D. P., Urdal, D. L., and Conlon, P. J. (1988) A short polypeptide marker sequence useful for recombinant protein identification and purification, *BioTechnology 6*, 1204−1210.

71. Scharf, S. J., G. T., H., and Erlich, H. A. (1986) Direct cloning and sequence analysis of enzymatically amplified genomic sequences, *Science 233*, 1076−1078.

72. Vallette, F., Mege, E., Reiss, A., and Adesnik, M. (1989) Construction of mutant and chimeric genes using the polymerase chain reaction, *Nucleic Acids Res. 17*, 723−733.

73. Yamazaki, T., Hinck, A. P., Wang, Y.-X., Nicholson, L. K., Torchia, D. A., Wingfield, P., Stahl, S. J., Kaufman, J. D., Chang, C.-H., Domaille, P. J., and Lam, P. Y. S. (1996) Three-dimensional solution structure of the HIV-1 protease complexed with DMP323, a novel cyclic urea-type inhibitor, determined by nuclear magnetic resonance spectroscopy, *Protein Sci. 5*, 495−506.

74. Meier, S., Häussinger, D., and Grzesiek, S. (2002) Charged acrylamide copolymer gels as media for weak alignment, *J. Biomol. NMR 24*, 351−356.

75. Ulmer, T. S., Ramirez, B. E., Delaglio, F., and Bax, A. (2003) Evaluation of backbone proton positions and dynamics in a small protein by liquid crystal NMR spectroscopy, *J. Am. Chem. Soc. 125*, 9179−9191.

76. Delaglio, F., Grzesiek, S., Vuister, G. W., Zhu, G., Pfeifer, J., and Bax, A. (1995) NMRPipe: a multidimensional spectral processing system based on UNIX pipes, *J. Biomol. NMR 6*, 277−293.

77. Goddard, T. D., and Kneller, D. G. SPARKY 3, University of California, San Francisco.

78. Yamazaki, T., Lee, W., Arrowsmith, C. H., Muhandiram, D. R., and Kay, L. E. (1994) A suite of triple resonance NMR experiments for the backbone assignment of ¹⁵N, ¹³C, ²H labeled proteins with high sensitivity, *J. Am. Chem. Soc. 116*, 11655−11666.

79. Bax, A., and Grzesiek, S. (1993) Methodological advances in protein NMR, *Acc. Chem. Res. 26*, 131−138.

80. Vuister, G. W., and Bax, A. (1993) Quantitative *J* correlation: A new approach for measuring homonuclear three-bond $J(H^NH^α)$ coupling constants in ¹⁵N-enriched proteins, *J. Am. Chem Soc. 115*, 7772−7777.

81. Ottiger, M., Delaglio, F., and Bax, A. (1998) Measurement of *J* and dipolar couplings from simplified two-dimensional NMR spectra, *J. Magn. Reson. 131*, 373−378.

82. Chou, J. J., Delaglio, F., and Bax, A. (2000) Measurement of one-bond ¹⁵N-¹³C′ dipolar couplings in medium sized proteins, *J. Biomol. NMR 18*, 101−105.

83. Grzesiek, S., and Bax, A. (1992) Improved 3D triple resonance NMR techniques applied to a 31 kDa protein, *J. Magn. Reson. 96*, 432−440.

84. Evenas, J., Mittermaier, A., Yang, D. W., and Kay, L. E. (2001) Measurement of ¹³Cα-¹³Cβ dipolar couplings in ¹⁵N,¹³C,²H-labeled proteins: Application to domain orientation in maltose binding protein, *J. Am. Chem. Soc. 123*, 2858−2864.

85. Farrow, N. A., Muhandiram, R., Singer, A. U., Pascal, S. M., Kay, C. M., Gish, G., Shoelson, S. E., Pawson, T., Forman-Kay, J. D., and Kay, L. E. (1994) Backbone dynamics of a free and a phosphopeptide-complexed Src homology 2 domain studied by ¹⁵N NMR relaxation, *Biochemistry 33*, 5984−6003.

86. Spera, S., Ikura, M., and Bax, A. (1991) Measurement of the exchange rates of rapidly exchanging amide protons: application to the study of calmodulin and its complex with myosin light chain kinase fragment, *J. Biomol. NMR 1*, 155−165.

87. Cornilescu, G., Delaglio, F., and Bax, A. (1999) Protein backbone angle restraints from searching a database for chemical shift and sequence homology, *J. Biomol. NMR 13*, 289−302.

88. Schwieters, C. D., Kuszewski, J. J., Tjandra, N., and Clore, G. M. (2003) The Xplor-NIH NMR molecular structure determination package, *J. Magn. Reson. 160*, 65−73.

89. Quina, F. H., Nassar, P. M., Bonilha, J. B. S., and Bales, B. L. (1995) Growth of sodium dodecyl sulfate micelles with detergent concentration, *J. Phys. Chem. 99*, 17028−17031.

90. Mesleh, M. F., Veglia, G., DeSilva, T. M., Marassi, F. M., and Opella, S. J. (2002) Dipolar waves as NMR maps of protein structure, *J. Am. Chem Soc. 124*, 4206−4207.

91. Krueger-Koplin, R. D., Sorgen, P. L., Krueger-Koplin, S. T., Rivera-Torres, I. O., Cahill, S. M., Hicks, D. B., Grinius, L., Krulwich, T. A., and Girvin, M. E. (2004) An evaluation of detergents for NMR structural studies of membrane proteins, *J. Biomol. NMR 28*, 43−57.

92. Palmer, A. G. (2004) NMR characterization of the dynamics of biomacromolecules, *Chem. Rev. 104*, 3623−3640.

93. Lipari, G., and Szabo, A. (1982) Model-free approach to the interpretation of nuclear magnetic resonance relaxation in mac-romolecules. 1. Theory and range of validity, *J. Am. Chem. Soc. 104*, 4546−4559.

94. Lipari, G., and Szabo, A. (1982) Model-free approach to the interpretation of nuclear magnetic resonance relaxation in mac-romolecules. 2. Analysis of experimental results, *J. Am. Chem. Soc. 104*, 4559−4570.

95. Chandra, S., Chen, X., Rizo, J., Jahn, R., and Sudhof, T. C. (2003) A broken α-helix in folded α-synuclein, *J. Biol. Chem. 278*, 15313−15318.

96. Clore, G. M., Szabo, A., Bax, A., Kay, L. E., Driscoll, P. C., and Gronenborn, A. M. (1990) Deviations from the simple two-parameter model-free approach to the interpretation of nitrogen-15 nuclear magnetic relaxation of proteins, *J. Am. Chem. Soc. 112*, 4989−4991.

97. Blackledge, M. (2005) Recent progress in the study of biomo-lecular structure and dynamics in solution from residual dipolar couplings, *Prog. Nucl. Magn. Reson. Spectrosc. 46*, 23−61.

98. Kontaxis, G., Delaglio, F., and Bax, A. (2005) Molecular fragment replacement approach to protein structure determination by chemical shift and dipolar homology database mining, *Methods Enzymol. 394*, 48−78.

99. Sass, J., Cordier, F., Hoffmann, A., Rogowski, M., Cousin, A., Omichinski, J. G., Lowen, H., and Grzesiek, S. (1999) Purple membrane induced alignment of biological macromolecules in the magnetic field, *J. Am. Chem. Soc. 121*, 2047−2055.

100. Louhivuori, M., Paakkonen, K., Fredriksson, K., Permi, P., Lounila, J., and Annila, A. (2003) On the origin of residual dipolar couplings from denatured proteins, *J. Am. Chem. Soc. 125*, 15647−15650.

101. Campbell, S. M., Crowe, S. M., and Mak, J. (2002) Virion-associated cholesterol is critical for the maintenace of HIV-1 structure and infectivity, *AIDS 16*, 2253−2261.
102. Guyader, M., Kiyokawa, E., Abrami, L., Turelli, P., and Trono, D. (2002) Role for human immunodeficiency virus type 1 membrane cholesterol in viral internalization, *J. Virol. 76*, 10356−10364.
103. Viard, M., Parolini, I., Sargiacomo, M., Fecchi, K., Ramoni, C., Ablan, S., Ruscetti, F. W., Wang, J. M., and Blumenthal, R. (2002) Role of cholesterol in human immunodeficiency virus type 1 envelope protein-mediated fusion with host cells, *J. Virol. 76*, 11584−11595.
104. Fisher, L. E., Engelman, D. M., and Sturgis, J. N. (1999) Detergents modulate dimerization, but not helicity, of the glyco-phorin A transmembrane domain, *J. Mol. Biol. 293*, 639−651.
105. Koradi, R., Billeter, M., and Wuthrich, K. (1996) MOLMOL: A program for display and analysis of macromolecular structures, *J. Mol. Graphics 14*, 51−55.
106. Laskowski, R. A., MacArthur, M. W., Moss, D. S., and Thornton, J. W. (1993) PROCHECK: A program to check the stereochem-ical quality of protein structures, *J. Appl. Crystallogr. 26*, 283−291.
107. Kay, L. E., Keifer, P., and Saarinen, T. (1992) Pure absorption gradient enhanced heteronuclear single quantum correlation spectroscopy with improved sensitivity, *J. Am. Chem. Soc. 114*, 10663−10665.
108. Palmer, A. G., Rance, M., and Wright, P. E. (1991) Intramolecular motions of a zinc finger DNA-binding domain from Xfin characterized by proton-detected natural abundance ^{13}C hetero-nuclear NMR spectroscopy, *J. Am. Chem. Soc. 113*, 4371−4380.
109. Mandel, A. M., Akke, M., and Palmer, A. G. (1995) Backbone dynamics of *Escherichia coli* ribonuclease HI: Correlations with structure and function in an active enzyme, *J. Mol. Biol. 246*, 144−163.
110. Baker, N. A., Sept, D., Joseph, S., Holst, M. J., and McCammon, J. A. (2001) Electrostatics of nanosystems: application to micro-tubules and the ribosome, *Proc. Natl. Acad. Sci. U.S.A. 98*, 10037−10041.
111. DeLano, W. L. (2002) The PyMOL Molecular Graphics System, DeLano Scientific, San Carlos, CA (http://www.pymol.org).

BI051672A